Title

Caenorhabditis elegans ALG-1 antimorphic mutations uncover functions for Argonaute in microRNA guide strand selection and passenger strand disposal

Journal

Proceedings of the National Academy of Sciences of the United States of America, 112(38)

ISSN

0027-8424

Authors

Zinovyeva, Anna Y
Veksler-Lublinsky, Isana
Vashisht, Ajay A
et al.

Publication Date

2015-09-22

DOI

10.1073/pnas.1506576112

Peer reviewed

Caenorhabditis elegans ALG-1 antimorphic mutations uncover functions for Argonaute in microRNA guide strand selection and passenger strand disposal

Anna Y. Zinovyeva[a,1], Isana Veksler-Lublinsky[a,1], Ajay A. Vashisht[b], James A. Wohlschlegel[b], and Victor R. Ambros[a,2]

[a]Program in Molecular Medicine, RNA Therapeutics Institute, University of Massachusetts Medical School, Worcester, MA 01605; and [b]Department of Biological Chemistry, David Geffen School of Medicine, University of California, Los Angeles, CA 90095

Edited by H. Robert Horvitz, Howard Hughes Medical Institute, Cambridge, MA, and approved August 14, 2015 (received for review April 3, 2015)

MicroRNAs are regulators of gene expression whose functions are critical for normal development and physiology. We have previously characterized mutations in a *Caenorhabditis elegans* microRNA-specific Argonaute ALG-1 (Argonaute-like gene) that are antimorphic [*alg-1(anti)*]. *alg-1(anti)* mutants have dramatically stronger microRNA-related phenotypes than animals with a complete loss of ALG-1. ALG-1(anti) miRISC (microRNA induced silencing complex) fails to undergo a functional transition from microRNA processing to target repression. To better understand this transition, we characterized the small RNA and protein populations associated with ALG-1(anti) complexes in vivo. We extensively characterized proteins associated with wild-type and mutant ALG-1 and found that the mutant ALG-1(anti) protein fails to interact with numerous miRISC cofactors, including proteins known to be necessary for target repression. In addition, *alg-1(anti)* mutants dramatically overaccumulated microRNA* (passenger) strands, and immunoprecipitated ALG-1(anti) complexes contained nonstoichiometric yields of mature microRNA and microRNA* strands, with some microRNA* strands present in the ALG-1(anti) Argonaute far in excess of the corresponding mature microRNAs. We show complex and microRNA-specific defects in microRNA strand selection and microRNA* strand disposal. For certain microRNAs (for example mir-58), microRNA guide strand selection by ALG-1(anti) appeared normal, but microRNA* strand release was inefficient. For other microRNAs (such as mir-2), both the microRNA and microRNA* strands were selected as guide by ALG-1(anti), indicating a defect in normal specificity of the strand choice. Our results suggest that wild-type ALG-1 complexes recognize structural features of particular microRNAs in the context of conducting the strand selection and microRNA* ejection steps of miRISC maturation.

Argonaute | ALG-1 | microRNA | microRNA* | passenger

MicroRNAs are small noncoding RNAs that, as part of a microRNA induced silencing complex (miRISC), bind to complementary sites in the 3′UTR of target messenger RNAs and cause translational repression or degradation of the target mRNA. microRNAs are predicted to posttranscriptionally regulate as much as 60% of mammalian protein coding genes (1), making them powerful regulators of physiological and developmental processes. Faithful microRNA biogenesis and programming of miRISC with the appropriate microRNA and accessory protein factors are essential for proper posttranscriptional gene regulation by microRNAs.

Mature ∼22-nt single-stranded microRNAs are generated and loaded into specialized Argonaute proteins [ALG-1 (Argonaute-like gene) and ALG-2 in *Caenorhabditis elegans*] through a series of enzymatic and RNA-protein assembly steps. First, the primary microRNA transcript is processed by the Drosha/Pasha microprocessor complex into a hairpin precursor and exported into the cytoplasm, where the RNAse III enzyme Dicer cleaves the precursor to generate a duplex, consisting of two short strands of RNA, corresponding to the "5p" and "3p" strands of the precursor hairpin. The microRNA duplex is then bound by Argonaute, such that one of the duplex strands (the eventual guide strand, or "miR" strand) becomes stably associated with Argonaute and the other strand (referred to as the passenger strand, or "miR*" strand) becomes discarded and degraded.

It is generally thought that the microRNA duplex is transferred to Argonaute in the context of a miRISC loading complex (miRLC), which contains Argonaute associated with Dicer (2, 3). The loading of the Argonaute with the duplex is also assisted by chaperone proteins Hsp70/Hsp90 (4–6).

Critical to proper miRISC assembly and subsequent microRNA-mediated gene repression is the accurate and consistent selection of which strand of the 5p/3p duplex will be loaded into Argonaute as the guide microRNA. This process of guide strand selection involves establishing the proper orientation of the duplex within the miRLC, followed by ejection and disposal of the passenger strand (7). For most microRNAs, guide strand selection is highly asymmetric and specific, so that either the 5p or the 3p accumulate in dramatic excess over the other (8, 9). This specificity of guide strand choice has been shown to be associated with certain features of the 5p::3p duplex: (*i*) The presence and configuration of centrally located mismatches for *Drosophila* microRNAs (10–12), (*ii*) the identity of the 5′ nucleotide of the guide microRNA (13–15), and (*iii*) the relative thermodynamic stability of the two ends of the miR::miR* duplex (16–18), which

Significance

Loading of Argonautes with the correct strand of the pre-miRNA duplex and disposal of the other strand are essential steps in microRNA biogenesis. Here we report characterization of the protein and microRNA populations associated with mutant ALG-1 Argonautes that are defective in transitioning from microRNA processing to target repression. We show that mutant Argonaute erroneously associates with the normally discarded microRNA* strands, signifying a role for Argonaute ALG-1 in microRNA strand selection. Accumulation of microRNA* is dependent on the microRNA identity, suggesting that specific microRNA features allow wild-type Argonautes to distinguish among different microRNAs. These findings are relevant to understanding Argonaute roles in microRNA biogenesis and, more broadly, to the functions of microRNAs in development and disease.

Author contributions: A.Y.Z. and V.R.A. designed research; A.Y.Z., A.A.V., and J.A.W. performed research; I.V.-L., A.A.V., and J.A.W. contributed new reagents/analytic tools; A.Y.Z. and I.V.-L. analyzed data; and A.Y.Z., I.V.-L., and V.R.A. wrote the paper.

The authors declare no conflict of interest.

This article is a PNAS Direct Submission.

Data deposition: The sequence reported in this paper has been deposited in the GEO database (accession no. GSE72659). Proteomic mass spectrometry data have been deposited to the ProteomeXchange Consortium via the MassIVE partner repository (data set identifier PXD002835).

[1]A.Y.Z. and I.V.-L. contributed equally to this work.

[2]To whom correspondence should be addressed. Email: ambrosvictor@gmail.com.

This article contains supporting information online at www.pnas.org/lookup/suppl/doi:10.1073/pnas.1506576112/-/DCSupplemental.

has a dramatic impact on strand choice in both flies and mammals. It should be noted that the relative thermodynamic stability of the duplex ends may be a primary determinant of strand selection for perfectly paired duplexes of siRNAs, but may be less important for the mismatched duplexes of most microRNAs (10, 11, 16, 17). Additionally, in *C. elegans*, microRNAs that produce 5p guides were reported to have similar thermodynamic stabilities of duplex ends as microRNAs that produce 3p guides (9), suggesting that at least in *C. elegans* other duplex features may be more important for strand selection (9). Features, such as microRNA duplex sequence composition and position of mismatches, could instead be major contributors to strand selection (19–21).

Although guide strand selection appears to be highly asymmetric for most microRNAs, for a small subset of microRNAs substantial quantities of both 5p and 3p strands can accumulate, and in at least some cases there is evidence for functional roles for both strands (22–25). It's possible that the relative loading of 5p and 3p strands as the guide could be regulated by upstream signals acting via Argonaute or other components of the miRLC. How *C. elegans* Dicer DCR-1 may contribute mechanistically to the specificity of microRNA loading and guide strand selection is unknown. Mammalian Dicer-associated proteins TRBP/PACT contribute to strand selection (26), and R2D2, a key component of *Drosophila* miRLC, is dispensable for miR strand selection (27). Interestingly, mammalian Dicer itself may be dispensable for asymmetric miRISC duplex loading, at least under certain circumstances (28, 29). The Argonaute protein itself may have the capacity to distinguish among specific microRNAs to determine the guide/miR vs. passenger/miR* fates of the 5p and 3p strands. Indeed, a very recent report has suggested a direct role for mAGO2 in miR strand choice (30). All these considerations emphasize the importance of acquiring a better understanding of the regulation of microRNA guide strand choice by Argonaute complexes in vivo.

We reported previously novel antimorphic alleles of the *C. elegans* Argonaute gene *alg-1* that broadly impair the functions of many microRNAs, apparently by sequestering microRNAs into immature and ineffectual miRLC complexes (31). The mutant ALG-1(anti) proteins exhibit an increased association with the miRLC component Dicer DCR-1 in vivo, and a decreased association with the miRISC effector AIN-1 (ALG-1 interacting protein-1). We proposed that ALG-1(anti)–containing complexes associate with microRNAs, but fail to properly mature from the Dicer-containing miRLCs to the effector miRISCs, thereby sequestering microRNAs in immature (and nonfunctional) RISC complexes (31). To better understand both the protein and the microRNA dynamics associated with this miRLC-to-miRISC maturation step, we further characterized the ALG-1(anti)–associated proteins and microRNAs using high-throughput proteomics and small RNAseq. Our results support the idea that *alg-1(anti)* mutants are defective in transitioning from biogenesis (miRLC) to effector (miRISC) status and identify conserved Argonaute-interacting proteins that may be specific to either miRLC or miRISC complexes. Moreover, our small RNAseq analysis shows that *alg-1(anti)* mutants accumulate miR* strands at levels dramatically greater than the wild-type, indicating that the ALG-1(anti) mutant proteins are defective in microRNA strand selection and miR* strand disposal. We show that the biogenesis of different microRNAs can be impacted very differently by ALG-1(anti). For example, in the case of mir-58, miR* strands are retained by the ALG-1(anti) Argonaute apparently as part of the miR::miR* duplex, suggesting defective miR* strand release. In contrast, for mir-2, the ALG-1(anti) complexes contained far more miR* strands than miR, indicating that miR-2 biogenesis suffers from defects in the strand selection step of miRISC maturation. These findings support a model wherein microRNA biogenesis and miRISC maturation involve critical roles for Argonaute both in recognizing features that define specific microRNAs and in exercising microRNA-specific programs of guide strand selection and miR* strand disposal.

Materials and Methods

***C. elegans* Culture and Genetics.** *C. elegans* culture was performed using standard nematode growth conditions (32), except the HB101 *Escherichia coli* strain was used as the food source. All strains were grown at 20 °C. Because of their strong heterochronic phenotypes, *alg-1(anti)* mutant animals often burst through the vulva during the L4-adult molt (31). Therefore, *alg-1(anti)* mutations were maintained in a *lin-31(n1053)* genetic background that impairs vulva development and thereby suppresses the bursting phenotype of *alg-1* mutants, while leaving their heterochronic phenotypes intact. The adult-specific *col-19::gfp* reporter transgene is also present in all of the strains. Therefore, the *alg-1(anti)* strains used here contain *lin-31; col-19::gfp*, and in all experiments the wild-type controls were *lin-31(n1053); col-19::gfp*.

Northern Blotting. Total RNA was isolated from mixed population of animals using TRIzol reagent (Life Technologies), and Northern blots were performed as previously described (33, 34). For oligo probe sequences please see *SI Materials and Methods*.

Firefly microRNA Quantifications. FirePlex microRNA assays were performed as previously described (31). For experiments involving 2′O-methyl oligonucleotide-mediated pull-down, equivalent fractions of input material and supernatant were tested using the FirePlex assays to quantitatively assess microRNA abundance in the starting material and microRNA depletion from the supernatant by the 2′-O-methylated oligonucleotide.

Small RNA Library Preparation and High-Throughput Sequencing. Small RNA cDNA libraries were prepared as previously described (35) and sequenced on the Illumina GAIIx instrument or the NextSeq500 (for L2 staged samples) using standard manufacturer's protocols.

Computational Analysis of cDNA Library Sequence Data. Detailed description of cDNA library sequence data analysis can be found in *SI Materials and Methods*.

ALG-1 Immunoprecipitation and Western Blot Analysis. Detailed description of antibodies, lysate preparation, immunoprecipitation, and Western blot analysis can be found in *SI Materials and Methods*.

2′O-Methyl Oligo Pull-Downs. The 2′O-methyl oligo pull-downs from extracts of whole worms were performed as described previously (36). For mass spectrometry, each sample contained 20 mg of total protein. Sequences of the 2′-O-methylated, biotinylated oligonucleotides can be found in *SI Materials and Methods*.

Mass Spectrometry Analysis of ALG-1 Immunopurified Complexes and 2′-O-Methyl Oligonucleotide Pulldown Complexes and Computational Analysis of Proteomic Data. For a detailed description of mass spectrometry analysis and computational analysis of ALG-1 associated proteomes, as well as data analysis of miR-58 and miR-58* associated proteins, see *SI Materials and Methods*.

Results

***alg-1(anti)* Mutant Phenotypes Correlate with a Shift in ALG-1–Associated Protein Complexes.** We reported previously that ALG-1(anti) protein showed a reduced interaction with the miRISC effector protein AIN-1 compared with wild-type ALG-1, and an increased association with Dicer, DCR-1 (31), suggesting an inability of ALG-1(anti)–containing miRISC to mature from processing complexes to effector complexes. To determine if interactions of ALG-1 with other proteins were affected by the *alg-1(anti)* mutations, we conducted ALG-1 IP from wild-type and *alg-1(anti)* animals followed by MudPIT (Multidimensional Protein Identification Technology) analysis to determine the composition of the associating complexes. The MudPIT data confirmed the results of our previous Western blot experiments, of a reduced ALG-1(anti) association with AIN-1 and an increased association with DCR-1 (Fig. 1*A* and Dataset S1), and also revealed a dramatic shift in the overall composition of the ALG-1(anti)–associated complexes (Datasets S1–S3). For example, 33 proteins were detected only in the immunoprecipitation (IP) of wild-type ALG-1, with 37 and 43 proteins detected only in the IP of ALG-1(ma192) and ALG-1(ma202), respectively. (Fig. 1*B*, Fig. S1, and Dataset S2). Consistent with the idea that ALG-1(anti) pre-miRISC complexes are defective in maturation from a

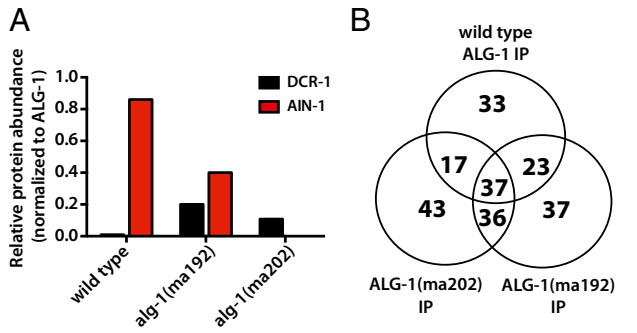

Fig. 1. Wild-type ALG-1 and ALG-1(anti) associate with distinct but overlapping protein populations. ALG-1 was immunoprecipitated from extracts of wild-type or *alg-1(anti)* animals using anti–ALG-1 antisera, and proteins were quantified by MudPIT proteomics, as described in *SI Materials and Methods*. (*A*) Association of AIN-1 with ALG-1(ma192) and ALG-1(ma202) is reduced compared with wild-type ALG-1, whereas association of DCR-1 with ALG-1(ma192) and ALG-1(ma202) is increased compared with wild-type ALG-1. AIN-1 and DCR-1 abundances in IPs are normalized to the abundance of ALG-1. (*B*) Venn diagram representation of the wild-type ALG-1–, ALG-1(ma192)–, and ALG-1(ma202)–associated proteins.

miRISC biogenesis stage to the mature effector miRISC complex, we observed that the ALG-1(anti) IP recovered an increased yield, compared with wild-type, of certain *hsp-60* and *hsp-70* family proteins and other putative chaperones (Datasets S1–S3), and a reduced yield of several known miRISC effector components, including the poly-A binding proteins PAB-1 and PAB-2 (Dataset S1), which have been shown to play critical roles in target repression (37 and 38; reviewed in ref. 39). This trend was seen across the two *alg-1(anti)* mutants examined: *alg-1(ma192)* and *alg-1(ma202)* (Fig. 1 and Dataset S1), which affect the PIWI and MID domains of the protein, respectively (31). ALG-1(ma192) and ALG-1(ma202) coimmunoprecipitated with overlapping yet nonidentical sets of proteins (Fig. 1, Fig. S1, and Dataset S1), consistent with the hypothesis that the two mutations may not have identical effects on the ability of ALG-1 to interact with various partners.

It should be noted that the proteins coimmunoprecipitated with ALG-1 in these experiments could include factors that directly interact with ALG-1 or that indirectly associate with miRISC by binding to target mRNAs, because our IP experiments were performed in the absence of RNase treatment.

***alg-1(anti)* Animals Accumulate miR* Strands and Precursor Hairpin Loops.** Given that ALG-1(anti) miRLC exhibits an apparent defect in maturing from a Dicer-containing configuration to the effector miRISC configuration, and considering that miR* strand release is expected to be associated with that maturation process, we tested whether *alg-1(anti)* mutants accumulate abnormal levels of miR* strands. Indeed, Northern blot analysis reveals a dramatic accumulation of the miR* strands for mir-80, mir-58, and mir-77 in *alg-1(anti)* mutants (Fig. 2*A*). Deep-sequencing of small RNA cDNA libraries from wild-type and *alg-1(anti)* mixed-staged animals confirmed that miR* strand accumulation occurs in *alg-1(anti)* mutants for most microRNAs, where in many cases the miR* strand increased many-fold in *alg-1(anti)* compared with wild-type (Fig. 2*B*). Moreover, *alg-1(anti)* mutants exhibited an increase (threefold, on average) in accumulation of the loop biproduct of the precursor microRNA processing (Fig. 2*C* and Fig. S2). MiR* strand accumulation occurred for most microRNAs regardless of the normal wild-type microRNA abundance (Fig. 2 *D* and *E*). For some microRNAs, such as mir-2 and mir-244, *alg-1(anti)* mutants showed an astounding miR*/miR ratio of 20–30, meaning that the passenger strand accumulated to levels 20- to 30-times greater than its microRNA counterpart (Table 1 and Dataset S4). This finding was in stark contrast to the wild-type, where the miR*/miR ratio was always less than one, and for most microRNAs rarely exceeded 0.02 (Table 1 and Dataset S4). Interestingly, the *alg-1(ma202)* allele affects miR* accumulation to a greater extent than does *alg-1(ma192)* (Fig. 2, Table 1, and Dataset S4), with little correlation between the profiles of miR* accumulation between the two alleles (Fig. S3). This finding is not surprising considering that *alg-1(ma192)* and *alg-1(ma202)* affect distinct domains of ALG-1.

To assess whether the *alg-1(anti)* miR*/miR ratio phenotype may be affected by developmental stage, we sequenced small RNA cDNA libraries from second larval-stage (L2) populations of wild-type and *alg-1(anti)* animals. L2 stage *alg-1(anti)* mutants were found to accumulate miR* strands many-fold compared with wild-type (Fig. S4 and Dataset S4), similarly to mixed-staged populations. Interestingly, microRNAs that showed a miR*/miR ratio of >1 in total RNA samples formed overlapping yet distinct groups in mixed-stage vs. L2 animals (Fig. S4). The differences observed could reflect differential microRNA tissue specificity and abundance at various stages of development. Importantly, however, a subset of microRNAs exhibited consistent miR*/miR ratios in both L2 and mixed-animals populations (Fig. S4 and Dataset S4).

Immunoprecipitated ALG-1(anti) Complexes Show an Increased Association with miR* Strands and Exhibit a Reversed Strand Bias for Some microRNAs. Because we observed the passenger microRNA strand accumulation in the *alg-1(anti)* animals, we hypothesized that these passenger strands may be bound to the ALG-1(anti) Argonaute. To address this question, we immunoprecipitated ALG-1 from wild-type and mutant mixed-staged animals and cloned and sequenced the associated small RNAs. The immunoprecipitated material was enriched for microRNA populations compared with the input (Fig. 3*A*) and was correspondingly de-enriched for other RNA populations (Fig. 3*B*). We found that immunoprecipitated ALG-1(anti) associated with greater quantities of miR* strands compared with the wild-type ALG-1 (Fig. 3*C*). In many cases, the miR*/miR ratios were clearly enriched in ALG-1 (ma202) IP compared with input (for example, for mir-77) (Table 1 and Dataset S4), supporting a specific association of those passenger strands with the ALG-1(anti) Argonaute. Interestingly, the immunoprecipitated ALG-1(anti) also showed an increased association with loop biproducts of precursor microRNA processing (Fig. 3*D*), suggesting that ALG-1(anti) miRISCs may be failing to completely eject both miR* and loop products after Dicer cleavage.

MiR* strand accumulation in ALG-1(anti) complexes appeared to occur for the majority of microRNAs regardless of their normal abundance (Fig. 3 *E* and *F*, Table 1, and Dataset S4), including very highly abundant microRNAs, such as mir-58 (Fig. 3*G* and Table 1). Depending on the microRNA, the ratio of miR* to miR in ALG-1(anti) complexes could vary across a wide range, and for most microRNAs the two strands associated with ALG-1(anti) nonstoichiometrically (Table 1 and Dataset S4). Notably, for some microRNAs, the miR* strand accumulated in ALG-1(anti) complexes to a greater extent than the corresponding miR strand (Table 1). For example, for mir-2, the miR-2* strand associated with ALG-1(anti) several-fold more than the miR-2 strand (Fig. 3*G* and Table 1). These cases of miR* strand accumulation in excess to miR strand seem to reflect that ALG-1(anti) proteins are defective in not only miR* strand disposal, but also in the normal specificity of the miR guide strand choice (Fig. 4*A* and Table 1).

The 2′O-Methyl Oligo-Mediated Pull-Down of mir-58 Family and mir-2 microRNAs from Wild-Type and *alg-1(anti)* Differentially Enriches for miRISC Components. As noted above, the accumulation of miR* strands in ALG-1(anti) immunoprecipitates could reflect failure to release miR* in the context of normal strand loading choice (Fig. 4*A*, model I) or an additional defect in strand choice (Fig. 4*A*, model II). According to model I, we expect to recover ALG-1(anti) (and perhaps other miRISC components) preferentially using an anti-miR oligo, but not with an anti-miR* oligo. In contrast, model II predicts that ALG-1(anti) and the associated

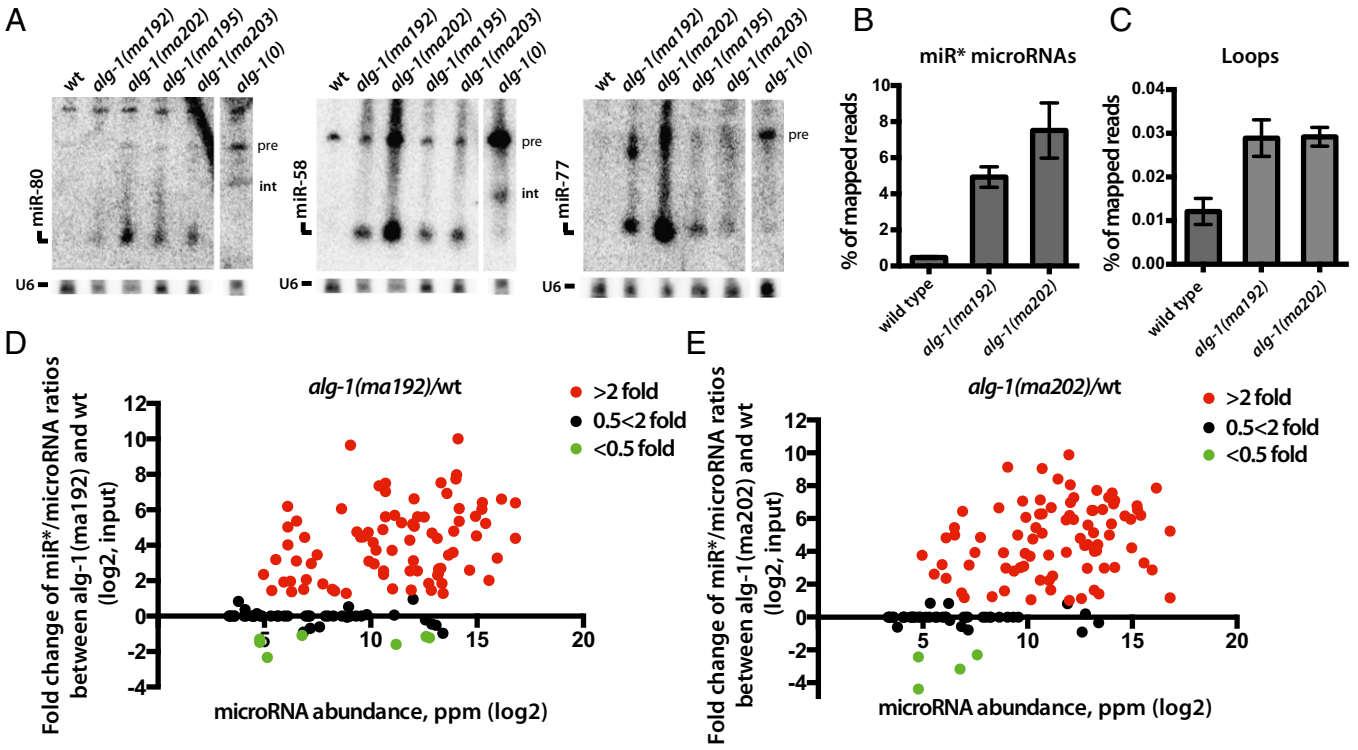

Fig. 2. *alg-1(anti)* mutants show an accumulation of miR* strands in total RNA. (*A*) Northern blot analysis of total RNA extracted from wild-type and alg-1 mutants using probes against miR* strands (pre, precursor microRNA; int, intermediate species of microRNA processing presumably containing the passenger strand and the loop). (*B* and *C*) Deep-sequencing analysis of small RNA populations from wild-type, *alg-1(ma192)* and *alg-1(ma202)* mutant animals shows an increase in miR* populations (*B*) and loop accumulation (*C*) in the *alg-1* mutants compared with wild-type. (*D* and *E*) Scatterplots showing fold-change in individual miR*/miR ratios between *alg-1(anti)* and wild-type total RNA. Increased miR*/miR ratio is seen in *alg-1(ma192)* (*D*) and *alg-1(ma202)* (*E*) mutants and is independent of microRNA abundance (ppm). Red dots represent microRNAs with an increased miR*/miR ratio in the *alg-1* mutant over wild-type of at least twofold; green dots represent miRNAs with a decreased miR*/miR ratio in the *alg-1* mutant compared with wild-type of at least twofold. Black dots represent no change in miR*/miR ratio in the *alg-1* mutants compared with wild-type.

miRISC components should be recovered both by anti-miR pull-down and by anti-miR* pull-down. To distinguish between these models for mir-58 family microRNAs, we examined complexes recovered from wild-type and *alg-1(ma192)* lysates by 2′O-methyl oligo-mediated pull-down followed by MudPIT analysis of the associated complexes. We observed that known miRISC components were recovered by pull-down using an anti–miR-58 oligo but were not detected after pull-down of miR-58* (Fig. 4*B*). Both the miR-58* and three members of the mir-58 family microRNAs were efficiently depleted from the extract by 2′O-methyl pull-down (Fig. 4*C*), presumably because of the sequence homology between the related microRNAs (Fig. 4*D*). Therefore, we do not believe that the low signals for miRISC proteins in the anti–miR-58* pull-down (Fig. 4*B*) can be explained by inefficient base pairing of passenger with anti–miR-58* oligo. Rather, we interpret this result to support model I, where mir-58 family microRNA passenger strand accumulation reflects retention of the passenger strand in duplexes with an ALG-loaded guide strand. This explains the recovery of both miR-58* and miR-58 by IP of ALG-1(anti) (Fig. 4 *E* and *G*) and the asymmetry of miRISC component recovery in pull-down of miR-58 vs. miR-58* (Fig. 4 *B* and *H*). We believe that the efficient recovery of both strands by oligo pull-down reflects efficient competition of the 2′-O-methyl oligos for their cognate microRNA strands in extracts under the condition of the pull-down experiment.

Incidentally, Western blot analysis of the material recovered by the 2′O-methyl pull-down of mir-58 family guide strands (Fig. 4*F*) is qualitatively consistent with the MudPIT proteomic analysis of the same samples (Fig. 4*B*). Both the Western blot and MudPIT showed reduced association of ALG-1(anti) with mir-58 family microRNAs. However, the signal for ALG-1(anti) appeared more reduced as detected by the Western blot compared with the wild-type than the MudPIT data indicate (Fig. 4 *B* and *F* and Fig. S5). This finding could in part reflect the fact that the protein abundances of the miRISC components and other factors, as determined by MudPIT analysis, were normalized to the amount of the microRNA present in the starting material, as well as the efficiency of the pull-down (Fig. 4*B*). Furthermore, if ALG-1 and ALG-2 protein yields (Fig. 4*B*) were recalculated using only peptides that were unique to each Argonaute (discarding the shared peptides; see *Materials and Methods*), the difference between ALG-1 abundance in wild-type vs. *alg-1(anti)* animal pull-downs increases from twofold to ~sixfold (Fig. 4*B*), thus becoming more consistent with the Western blot data. However, it remains possible that ALG-1(anti) detection on a Western blot by the anti–ALG-1 antibody is hampered for unknown technical reasons. Another MudPIT/Western blot discrepancy, the presence of ALG-1 in the miR-58*-associated material as detected by Western blotting in wild-type (Fig. 4*F*), could be a result of the more stringent washing of the 2′-O-methyl pull-down material in preparation for the MudPIT analysis.

Curiously, although the miR-58 family miR strand pull-down from *alg-1(anti)* animals yielded a decreased recovery of ALG-1 compared with the wild-type ALG-1, an increased amount of ALG-2 was recovered, in addition to the RDE-1 Argonaute (Fig. 4*B* and Fig. S5). This finding suggests a possible reapportioning of some of the mir-58 family microRNAs in *alg-1(anti)* mutants that normally associate with ALG-1 into ALG-2 and perhaps other Argonautes. Consistent with this scenario, we did not detect a decrease in association of mir-58 family microRNAs with the miRISC effector protein AIN-1 (Fig. 4 *B* and *F* and Fig. S5), suggesting that at least a portion of the microRNAs must be in

Table 1. microRNAs classified according to their miR*/miR ratio in input or ALG-1 IPs from *alg-1(anti)* mutants and wild-type

		Wild-type				*alg-1(ma192)*				*alg-1(ma202)*				Fold-change in miR*/miR ratios between ALG-1(ma202) IP and ALG-1(wt) IP
		Average microRNA abundance (ppm)		Average miR*/miR ratio		Average microRNA abundance (ppm)		Average miR*/miR ratio		Average microRNA abundance (ppm)		Average miR*/miR ratio		
Class	mir	Input	IP	Input	IP	Input	IP	Input	IP	Input	IP	Input	IP	
Class I:	mir-244	335	336	0.149	0.068	1,644	467	0.762	0.937	132	52	21.024	21.700	321
Asymmetric	mir-87	297	327	0.102	0.005	258	181	2.400	1.081	158	94	13.566	9.205	1,942
(IP miR*/miR > 1)	mir-2	518	966	0.091	0.020	1,308	3,748	3.520	0.484	140	442	30.950	4.261	212
	mir-86	3,622	4,019	0.006	0.002	3,073	6,598	0.216	0.112	1,206	1,407	5.593	2.496	1,005
	mir-252	310	1,187	0.006	0.002	129	1,618	4.769	0.526	240	1,024	3.349	1.565	818
	mir-241	2,460	2,454	0.016	0.007	746	470	0.460	0.491	524	262	1.206	1.559	218
	mir-45	2,269	1,868	0.014	0.006	6,359	2,322	0.010	0.014	10,737	6,100	1.298	1.127	183
Class II:	mir-235	998	5,019	0.022	0.003	821	6,086	2.879	0.416	453	2,528	11.603	0.487	192
Asymmetric	mir-90	2,323	13,937	0.054	0.002	4,580	11,900	0.316	0.022	1,572	8,970	3.301	0.256	105
(input	mir-54	20,260	26,474	0.012	0.003	11,576	30,654	0.140	0.017	4,804	14,626	1.818	0.330	112
miR*/miR > 1)	mir-786	329	314	0.139	0.051	2,067	2,586	0.149	0.037	167	118	1.188	0.373	7
	mir-79	3,644	2,092	0.011	0.012	15,606	12,644	0.238	0.159	8,892	6,286	1.024	0.607	51
Class III:	mir-793	843	710	0.001	0.000	688	439	0.104	0.040	613	447	0.350	0.214	492
Accumulated	mir-77	34,022	14,471	0.002	0.001	19,458	18,383	0.114	0.063	53,246	27,746	0.190	0.467	463
	mir-67	4,987	4,783	0.002	0.001	3,705	4,158	0.197	0.197	3,536	5,558	0.533	0.336	457
	mir-82	23,791	24,879	0.001	0.000	7,637	5,013	0.065	0.010	18,774	19,543	0.133	0.057	213
	mir-64	16,189	18,788	0.000	0.000	3,522	8,989	0.077	0.008	13,263	16,721	0.087	0.027	170
	mir-1	68,107	82,018	0.002	0.000	13,608	6,031	0.183	0.065	29,357	26,087	0.202	0.068	160
	mir-43	1,365	580	0.012	0.006	3,638	791	0.232	0.291	5,604	1,702	0.716	0.833	136
	mir-50	9,314	10,552	0.004	0.001	2,792	1,126	0.151	0.017	698	659	0.564	0.087	134
	mir-52	61,157	45,748	0.001	0.000	112,055	286,661	0.131	0.017	35,070	49,065	0.312	0.057	131
	mir-792	217	186	0.003	0.002	111	119	0.071	0.082	53	50	0.286	0.237	125
	lin-4	28,721	34,049	0.000	0.000	12,529	3,248	0.438	0.083	9,432	5,610	0.051	0.003	114
	mir-248	267	314	0.001	0.000	122	84	0.104	0.033	61	49	0.066	0.028	113
	mir-58	99,377	86,512	0.003	0.002	186,421	106,646	0.066	0.162	75,670	48,452	0.119	0.205	112
	mir-38	4,656	2,615	0.007	0.001	12,010	1,343	0.025	0.014	6,628	1,940	0.142	0.129	95
	mir-1829c	458	385	0.007	0.001	568	718	0.011	0.017	138	113	0.024	0.067	92
	mir-84	7,428	8,996	0.004	0.001	5,116	3,399	0.097	0.029	11,952	14,754	0.184	0.063	92
	mir-81	24,466	27,301	0.001	0.000	7,395	8,512	0.190	0.013	15,353	28,579	0.142	0.012	84
	mir-74	3,845	2,478	0.001	0.000	6,947	2,253	0.005	0.002	2,180	1,301	0.043	0.009	79
	mir-71	54,306	58,135	0.009	0.003	34,269	18,007	0.354	0.206	29,816	28,479	0.688	0.248	78
	mir-55	39,420	39,856	0.001	0.000	37,619	77,519	0.047	0.002	19,635	35,531	0.059	0.006	75
Class IV:	mir-259	1,321	1,470	0.005	0.004	1,013	2,108	0.130	0.020	544	816	0.072	0.018	4
Unaffected	mir-250	6,847	1,897	0.013	0.002	10,518	2,811	0.007	0.005	24,762	9,243	0.010	0.009	4
	mir-1829a	71	136	0.284	0.030	49	92	1.107	0.108	43	74	0.506	0.096	3
	mir-356b	53	96	0.047	0.021	24	60	0.431	0.141	45	114	0.291	0.064	3
	mir-59	105	53	0.010	0.016	564	182	0.028	0.032	529	151	0.010	0.047	3
	mir-63	2,915	2,920	0.034	0.017	1,520	999	0.035	0.013	3,177	4,966	0.105	0.041	2
	mir-61	1,652	848	0.003	0.002	2,693	1,119	0.008	0.005	1,637	1,117	0.013	0.005	2
	mir-36	1,492	468	0.105	0.027	9,510	2,694	0.047	0.027	13,420	6,710	0.056	0.057	2
	mir-230	355	285	0.202	0.093	409	328	0.195	0.089	466	762	0.612	0.190	2
	mir-2214	189	84	0.021	0.112	403	148	0.056	0.202	617	151	0.050	0.220	2
	mir-4816	97	57	0.073	0.021	124	54	0.210	0.038	133	112	0.202	0.037	2
	mir-75	3,038	2,426	0.044	0.026	4,394	5,836	0.107	0.072	29,063	89,083	0.117	0.044	2
	mir-65	30,192	20,108	0.000	0.000	5,417	4,792	0.005	0.001	24,775	43,527	0.001	0.000	2
	mir-62	486	485	0.244	0.018	1,397	478	0.123	0.027	1,070	928	0.075	0.021	1
	mir-791	47	364	0.797	0.117	37	422	2.076	0.076	45	221	0.694	0.053	0
	mir-34	3,106	3,459	0.084	0.054	2,950	1,253	0.233	0.096	4,709	1,753	0.149	0.023	0

Class I: Asymmetric. MicroRNAs that had a miR*/miR ratio >1 in ALG-1(ma202) IP. Class II: Asymmetric in input. MicroRNAs that had a miR*/miR ratio >1 in input for the ALG-1(ma202) IP. Class III: Accumulated. 20 microRNAs representative of the microRNAs whose miR*/miR ratio was significantly increased in ALG-1(ma202) IP compared with wild-type ALG-1 IP. See Dataset S4 for a complete list. Class IV: Unaffected. MicroRNAs whose miR*/miR ratio changed ≤4 between wild-type ALG-1 IP and ALG-1(ma202) IP. ppm, parts per million.

miRISCs that contain AIN-1. The observed AIN-1 and DCR-1 signal (Fig. 4*F*) is likely to at least in part reflect complexes of miR-58 with ALG-2. Similar observations were made for the mir-52 family microRNA pull-downs (Fig. S6). Interestingly, mir-58 family microRNA association with AIN-2 was not observed in *alg-1(ma192)* mutant animals (Fig. 4*B*), suggesting that AIN-2 may differ from its homolog AIN-1 with respect to its interaction with Argonautes ALG-1 and ALG-2.

To understand the basis for miR-2* strand accumulation (Figs. 3*G*, 4*A*, and 5*A*) we conducted 2′O-methyl pull-down experiments from wild-type and *alg-1(anti)* animals using oligos complementary to miR-2 and miR-2* strands. Pull-down against miR-2 recovered ALG-1 protein from both wild-type and *alg-1(anti)* animals (Fig. 5*B*). Surprisingly, we found that pull-downs with an oligo complementary to the miR-2* also recovered ALG-1(anti) protein (Fig. 5*B*). This finding suggests that at least a subpopulation of miR-2* strands are associated with the mutant ALG-1(anti) as single strands, indicating that ALG-1(anti) is defective in proper strand selection for mir-2 (model II in Fig. 4*A*). This cannot be the only defect in miR-2::ALG-1(anti) association, because the quantity of ALG-1(anti) detected in the anti-miR-2* pull-down is less than what is associated with the miR-2 strand, even though miR-2* is in excess to miR-2 (Fig. 5*A*). This finding indicates that perhaps miR-2* strand accumulation in ALG-1(anti) complexes reflects a combination of two defects: its inefficient ejection from the duplex (model I in Fig. 4*A*) as well as erroneous miR-2* incorporation into the ALG-1(anti) Argonaute as guide (Fig. 4*A*, model II, and Fig. 5 *C* and *D*). However, miR-2 complementary 2′-O-methylated oligo cross-reacts with other members of the mir-2 family, given the sequence overlaps between family members, whereas miR-2* complementary oligo is expected to specifically recover miR-2*. These differential specificities of oligos may also contribute to the differing amount of ALG-1 observed as associated with both the mir-2 family microRNAs and miR-2* alone (Fig. 5 *A* and *B*).

The Set of microRNAs Exhibiting Grossly Abnormal miR* Loading by ALG-1(anti) Are Not Easily Distinguished by Features of Their microRNA Duplex Structures. None of class I asymmetric microRNAs (Table 1) are particularly enriched (relative to the other classes; see Table 1) for microRNAs that preferentially associate with ALG-1 compared with ALG-2 (40), suggesting that a simple bias of microRNAs to preferentially load into one Argonaute vs. another cannot explain the asymmetric miR* loading into ALG-1(anti). In addition, class I asymmetric microRNAs do not have a 5′ nucleotide bias for either miR or miR* (Fig. S7 *A* and *B*). Similarly, no 5p vs. 3p precursor arm bias was detected for asymmetric microRNAs (class I) compared with other classes (Table 1 and Fig. S7*C*). MicroRNAs with highly ALG-1(anti)–enriched miR* strands (class I in Table 1) also showed similar distribution of duplex and duplex end energies compared with those microRNAs whose miR* strands were not enriched in ALG-1 IP (classes II, III, and IV in Table 1, and Fig. S7 *D* and *E*). Pairing (or lack thereof) of the 5′ nucleotide of miR or miR* also does not explain the differential incorporation of some miR* strands into ALG-1(anti) (Fig. S7 *E* and *F*). Similarly, our analysis of differences between duplex seed energies on the 5′ end of the guide vs. 5′ end of the miR* (ΔΔG seed) did not distinguish the asymmetrically loaded microRNAs from the other classes (Fig. S7*G*).

Discussion

Here we report detailed molecular characterizations of the previously genetically described antimorphic *alg-1* mutations (31). These mutations were shown to have broad effects on microRNA function and are more detrimental than complete loss of ALG-1, yet do not significantly affect Dicer processing of microRNA precursors or mature guide microRNA accumulation (31). The strong phenotypes caused by ALG-1(anti) could be explained by the observation that ALG-1(anti) complexes contain microRNAs, but poorly associate with the miRISC effector AIN-1, and hence sequester microRNAs in ineffective complexes (31). Previous findings also showed that ALG-1(anti) complexes are more enriched for Dicer than are wild-type ALG-1 complexes, further indicating that ALG-1(anti) proteins could be defective in transition from miRISC biogenesis to miRISC function (31).

In this study, we aimed to better understand the effects of these *alg-1(anti)* mutations on ALG-1 function through comprehensive analysis of the profile of proteins and microRNAs associated with ALG-1(anti) complexes in vivo. MudPIT mass spectometry characterization of ALG-1(anti)–associated proteins revealed a shift in the profile of protein interactors compared with the wild-type that is consistent with defective miRISC maturation by ALG-1(anti). Furthermore, we show that for most microRNAs the ALG-1(anti) complexes inappropriately retain the miR* strand, the strand of the pre-microRNA duplex that is ordinarily, in the wild-type, chosen as the passenger strand and hence disposed of. In some cases, the miR* strand accumulates in dramatic excess to the microRNA strand, revealing defects in the specificity of guide strand choice.

These results suggest that the normal function of ALG-1 includes direct or indirect roles in (*i*) the specificity of the microRNA strand selection, and (*ii*) the disposal of the miR* strands. Importantly, we observe that the effects of ALG-1(anti) on microRNA strand selection and miR* disposal can differ widely—qualitatively and quantitatively—depending on the particular microRNA. This finding suggests that wild-type ALG-1 Argonaute normally functions as an active component of complexes that recognize specific microRNA precursors in such a way as to determine the specificity of microRNA strand selection and the efficiency of miR* strand disposal.

ALG-1(anti) Complex Composition Is Consistent with Stalled miRLC Complexes. Our MudPIT analysis of the ALG-1 coimmunoprecipitates from wild-type and *alg-1(anti)* mutant animals revealed a shift in the profile of ALG-1–associated proteins (Fig. 1, Fig. S1, and Dataset S1). This shift includes the detection of protein populations associated with ALG-1(anti) that were not detected in wild-type ALG-1 complexes, and an absence of proteins that were detected only in wild-type complexes. This finding is consistent with the model that both ALG-1(ma192) and ALG-1(ma202)-containing complexes are defective in properly maturing into functional miRISC. These MudPIT data support and expand our previous findings from Western blot analyses of Dicer and AIN-1 association with ALG-1(anti) (31). By MudPIT, ALG-1(anti) are observed to associate more with DCR-1 and less with AIN-1, than does wild-type ALG-1 (Fig. 1*A* and Dataset S1). The MudPIT data further show that ALG-1(anti) exhibit a reduced association with a set of additional proteins known to be required for microRNA target translational repression and target degradation, including poly(A)-binding proteins PAB-1 and PAB-2. At the same time, ALG-1(ma192) IPs contained an increase in heat-shock family proteins that have been previously shown to assist in the loading of the Argonautes (4, 6). Therefore, this observation further supports our model that ALG-1(anti)–containing complexes are stalled in a pre-miRISC form, perhaps as the miRLC.

Our deep-sequencing of cDNA libraries prepared from ALG-1(anti) immunoprecipitated complexes further supports the interpretation of ALG-1(anti) complexes as being stalled in a miRLC form. Notable in this regard is our finding that both miR* and loop sequences, which are excised by Dicer from microRNA precursors and usually ejected before miRISC maturation, are enriched in ALG-1 IP from *alg-1(anti)* worms compared with the wild-type (Fig. 3).

microRNAs Can Shift from ALG-1 to Other Argonautes in *alg-1(anti)* Animals. MudPIT analysis of complexes recovered by oligonucleotide-mediated pull-down of mir-58 family microRNAs from *alg-1(anti)* worm extracts revealed an increase in the amount of ALG-2 recovered (Fig. 4*B*). This increase could reflect an up-regulation of ALG-2 protein abundance in the *alg-1(anti)* background (for example, via a hypothetical compensatory regulation of ALG-2). We showed previously that *alg-2* mRNA levels were not detectably increased in *alg-1(anti)* animals, but we were not able to determine ALG-2 protein abundance because of a lack of ALG-2–specific antiserum (31). Alternatively, inability of ALG-1(anti) Argonautes to appropriately load miR-58 may result in a release of the mir-58 duplex from ALG-1(anti) and subsequent take up by the available microRNA competent Argonautes such as ALG-2 and RDE-1, according to a previously proposed "duplex sorting" model (11).

Interestingly, oligonucleotide-mediated pull-down of the miR-58 family guide also showed a relatively minor, but nevertheless

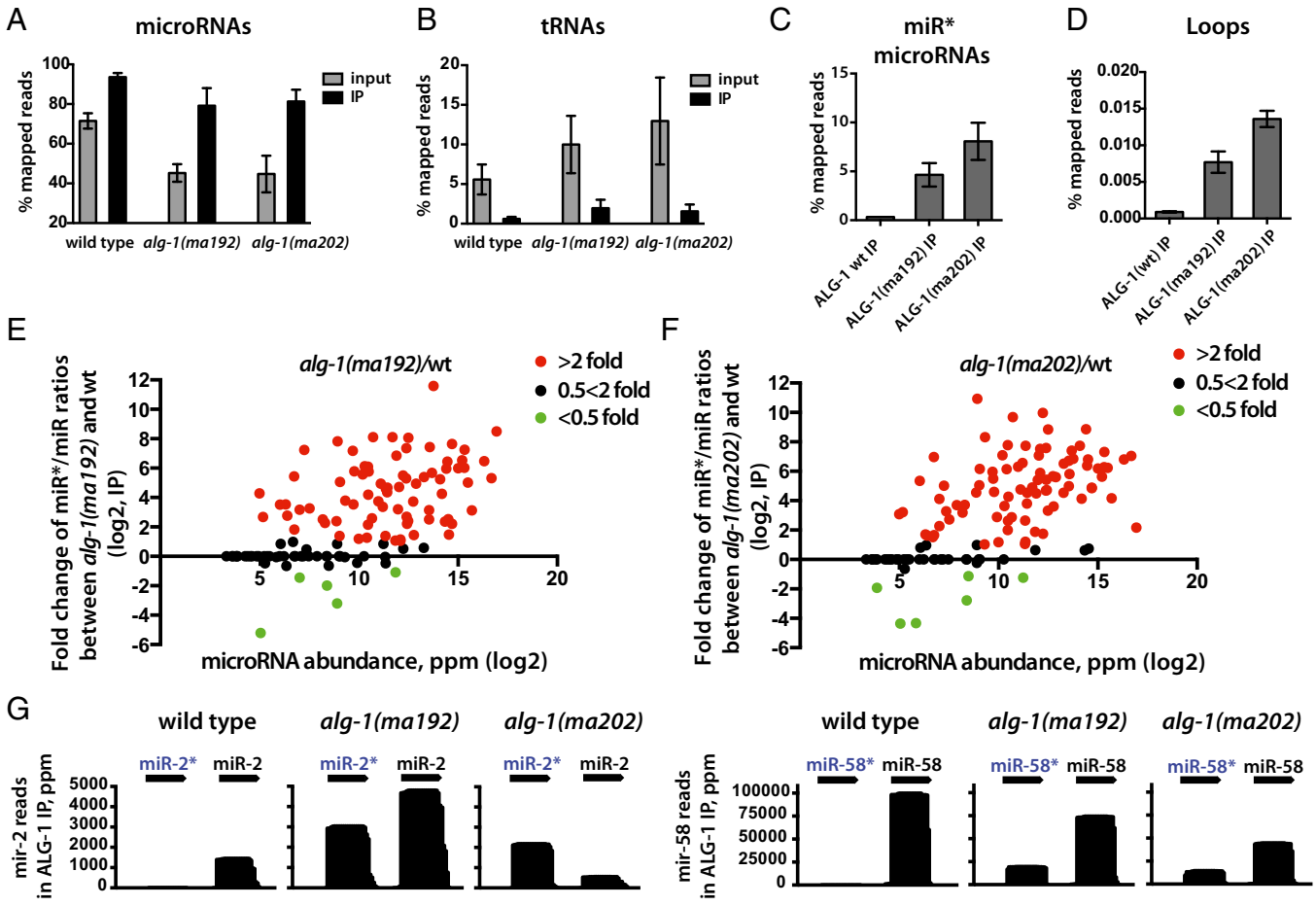

Fig. 3. ALG-1(anti) Argonaute associates with miR* strands to a much greater degree than does wild-type ALG-1. (*A* and *B*) microRNAs are enriched (*A*), and tRNAs are de-enriched (*B*) in the ALG-1 IP compared with input. (*C* and *D*) ALG-1(anti) associates with a greater amount of miR* strands (*C*) and precursor microRNA loops (*D*) compared with the wild-type ALG-1. (*E* and *F*) Scatterplots showing fold-change in individual miR*/miR ratios in material coimmunoprecipitates with ALG-1 from *alg-1(anti)* and wild-type. Increased miR*/miR ratio for microRNAs associated with ALG-1 is exhibited *for alg-1(ma192)* (*E*) and *alg-1(ma202)* (*F*) mutants and is independent of microRNA abundance. Red dots represent miRNAs with an increased miR*/miR ratio in the *alg-1* mutant over wild-type by at least twofold; green dots represent miRNAs with a decreased miR*/miR ratio in the *alg-1* mutant compared with wild-type of at least twofold. Black dots represent no change in miR*/miR ratio in *alg-1* mutants compared with wild-type. (*G*) Histograms showing miR-2 and miR-2*, as well as miR-58 and miR-58* strand association with immunoprecipitated wild-type and mutant ALG-1 protein.

striking, shift of these microRNAs to RDE-1 in *alg-1(anti)* mutants (Fig. 4*B* and Fig. S5). RDE-1 has been previously shown to associate with multiple classes of small RNAs, including microRNAs (41). It is possible that RDE-1 may function as a natural reservoir for microRNAs that are, under certain circumstances, excluded from ALG-1 and ALG-2. It is worth noting that if there were a broad shift in microRNAs from ALG-1(anti) to other Argonauts, then that could result in a general mitigation of the *alg-1(anti)* phenotypes by providing some measure of functional replacement of the defective ALG-1(anti) protein.

ALG-1(anti) Causes Defects in Guide Strand Choice and Passenger Strand Disposal. Ordinarily, for the majority of microRNA precursors, one strand of the duplex is specifically selected to associate with Argonaute in the guide strand configuration, whereas the other strand is ejected and subsequently degraded. Therefore, in the wild-type, the miR*/miR ratio is exceedingly small for most microRNAs, with few exceptions, such as mir-30 in mammals (42) and mir-47 in *C. elegans* (Dataset S4). A striking aspect of our findings is that the usual asymmetry of miR vs. miR* accumulation is dramatically altered in ALG-1(anti) complexes (Table 1). In ALG-1(ma202) complexes, 75 microRNAs exhibited a 4- to ~2,000-fold increase in the ratio of miR* to miR compared with the wild-type (Table 1 and Dataset S4).

Importantly, for certain microRNAs, the miR* strand accumulated in ALG-1(anti) complexes to levels in excess to their miR strand counterparts [for example, miR-2* in *alg-1(ma202)*]. In such cases of miR* excess, at least a portion of the miR*, must be loaded into ALG-1(anti) in the guide strand configuration. This interpretation is supported by our finding that oligonucleotide pull-down of miR-2* from *alg-1(ma202)* extracts yielded ALG-1, as detected by Western Blot (Fig. 5). Thus, for at least some microRNAs (class I in Table 1), ALG-1(anti) complexes fail to execute the proper specificity of guide strand choice.

For those microRNAs whose miR* strand did accumulate in ALG-1(anti) complexes, but not in excess to the microRNA strand (classes II and III in Table 1), the underlying defect could be a defective guide strand choice selection, although less potent than for the class I microRNAs. Alternatively, for some of these class II/III microRNAs, miR* strand accumulation could reflect simply a miR* strand release defect in the context of normal strand choice. Pull-down of miR-58* strands in *alg-1(anti)* did not appreciably recover ALG-1, ALG-2, AIN-1/2, or DCR-1 (Fig. 4 *B* and *F*), whereas pull-down of the miR-58 strand did recover these known Argonaute complex components (Fig. 4 *B* and *F*). Thus, unlike miR-2, where oligonucleotide pull-down of the miR* strand did yield ALG-1 (Fig. 5), the miR-58* strand seems to be not directly associated with ALG-1 but in a duplex

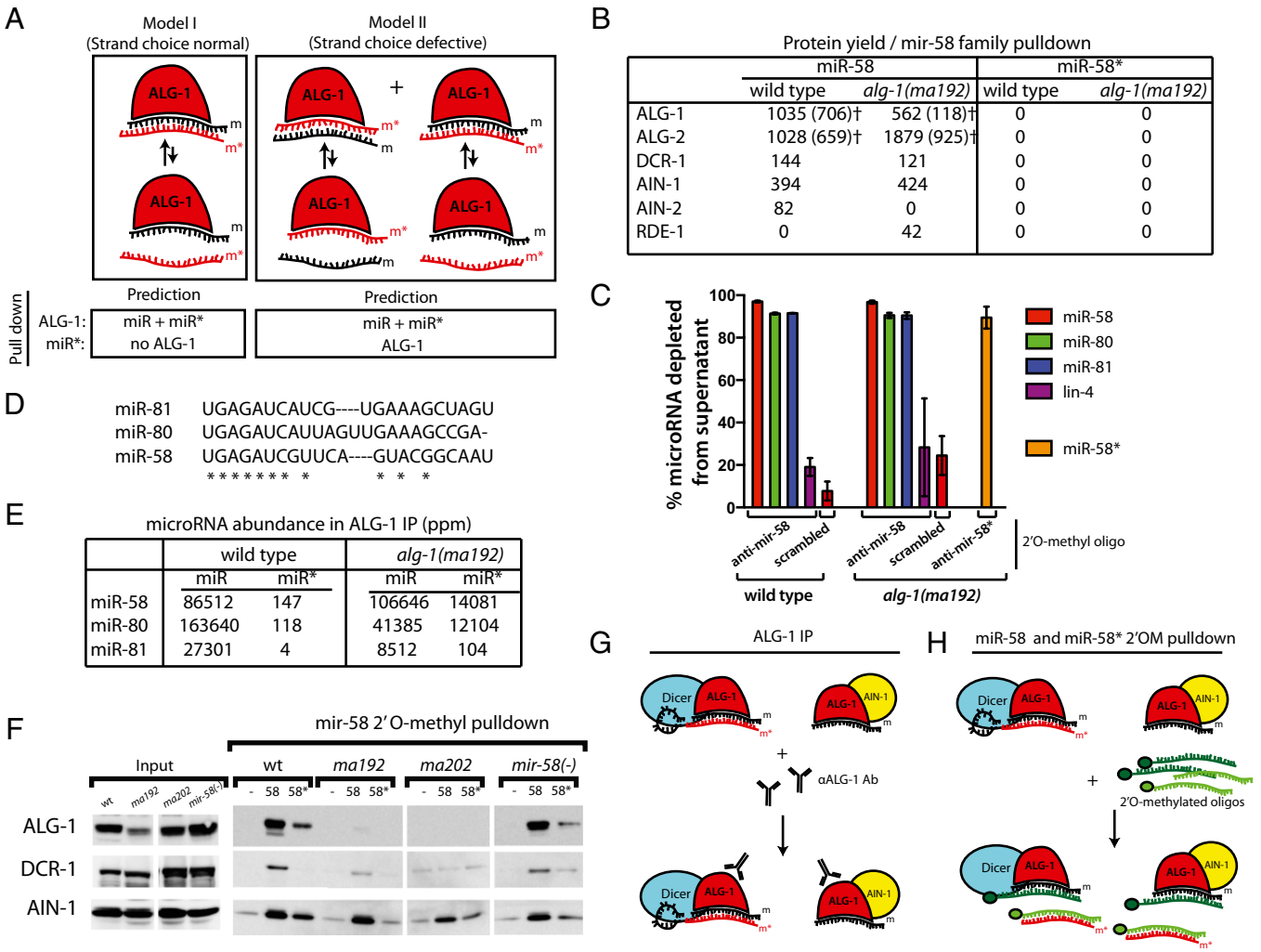

Fig. 4. 2′O-methyl oligonucleotide pull-downs from wild-type and *alg-1(anti)* mutants suggest that miR-58* accumulation in ALG-1 is a result of failure of ALG-1(anti) to release it from the duplex. (*A*) Two models for miR* microRNA accumulation in *alg-1(anti)* mutant animals. Model I: ALG-1(anti) complexes retain both microRNA strands primarily in a bound duplex. Model II: ALG-1(anti) complexes contain single strands of miR and miR* microRNAs because of a loss in the ability of the protein to differentiate between the two strands. Predictions of the outcome for IP and pull-down experiments are shown directly below each model. (*B*) Protein yield of miRISC components and other small RNA related factors from mir-58 family microRNA pull-down as determined by MudPIT proteomics and normalized to the amount of RNA depleted by the 2′O-methyl pull-down. †ALG-1 and ALG-2 protein yield as determined based on normalized spectral abundance factor $(NSAF)_{unique}$ (*SI Materials and Methods*). (*C*) Efficiency of the miR-58 and miR-58* strand pull-downs presented as percent microRNA depleted from the supernatant in samples shown in *B*. (*D*) Sequence alignments between members of the mir-58 family of microRNAs. (*E*) miR-58 family microRNA and miR* abundances in wild-type ALG-1 and ALG-1(anti) IP. (*F*) Western blot analysis of mir-58 microRNA family pull-downs from extracts of *alg-1(anti)* and wild-type animals showing association of ALG-1, DCR-1, and AIN-1 with mir-58 family microRNAs (-, scrambled oligo control; 58, oligo against miR-58; 58*, oligo against miR-58*). (*G* and *H*) Summary model for the miR-58* strand and related proteins accumulation as observed in *alg-1(anti)* mutants by (*G*) ALG-1(anti) IP and (*H*) miR-58 and miR-58* 2′O-methyl pull-downs (m, miR; m*, miR*).

with ALG-bound miR-58 microRNA. This finding indicates that for mir-58 and likely many other microRNAs exhibiting miR* strand accumulation, ALG-1(anti) causes a miR* strand release defect (Fig. 4*A*, model I).

Defective passenger strand release by ALG-1(anti) suggests an active role for ALG-1 in the passenger release process. This role may represent a direct activity of ALG-1, such as cleavage of passenger strand by ALG-1 slicer activity. However, recombinant ALG-1(anti) protein seems to retain slicer activity by in vitro assays (31). Moreover, many microRNA precursors contain mismatched bases in the center of their precursor helix, precluding passenger strand slicing (43). Thus, excess miR* accumulation in ALG-1(anti) Argonautes likely reflects passenger release by slicing-independent mechanisms.

It is curious that for certain microRNAs we observed high levels of miR* strands in whole-worm extracts, yet the miR* strands of those particular microRNAs were not efficiently recovered by in ALG-1 immunoprecipitation (Fig. 4*B* and Table 1). This finding suggests that many miR* strands are either not stably associated with ALG-1 under the conditions of IP, or they are associated with other complexes of unknown composition.

Throughout our characterizations of the *alg-1(anti)* mutants we observed quantitative and qualitative differences between *alg-1(ma192)* and *alg-1(ma202)* alleles in how these two mutant ALG-1 proteins affect miR* strand accumulation for specific microRNAs. *alg-1(ma202)* animals appear to accumulate miR* strands to a greater degree than do *alg-1(ma192)* mutants, both in total RNA samples and in ALG-1 IP (Figs. 2 and 3, Table 1, and Fig. S3). *alg-1(ma192)* and *alg-1(ma202)* alleles affect two distinct domains of ALG-1 (PIWI and MID, respectively) and may differentially affect ALG-1 interactions with specific microRNAs and protein cofactors. It is intriguing to consider that the two mutated forms of

A

microRNA abundance in ALG-1 IP (ppm)

	wild type		*alg-1(ma192)*		*alg-1(ma202)*	
	miR	miR*	miR	miR*	miR	miR*
miR-2	966	17	3748	1973	442	1837
miR-43	580	3	791	210	1702	1147
miR-250	1897	4	2811	15	9243	79
miR-797	417	1	364	5	237	10

B

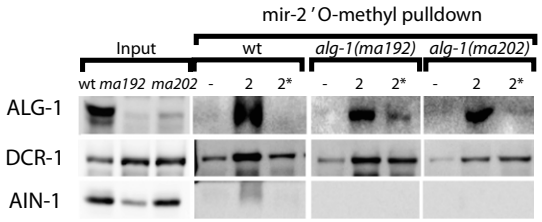

C

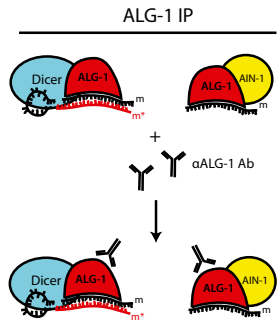

D

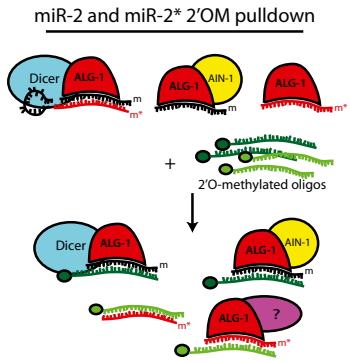

Fig. 5. 2′-O-methyl oligonucleotide pull-downs from wild-type and *alg-1(anti)* mutants suggest that miR-2* accumulation in ALG-1 is in part a result of inappropriate loading into the ALG-1(anti) Argonaute. (*A*) mir-2 family microRNA and miR* abundances in wild-type ALG-1 and ALG-1(anti) IP. (*B*) Western blot analysis of miR-2 and miR-2* pull-downs from extracts of *alg-1(anti)* and wild-type animals showing association of ALG-1, DCR-1, and AIN-1 with mir-58 family microRNAs (-, scrambled oligo control; 2, oligo against miR-2; 2*, oligo against miR-2*). (*C* and *D*) Summary model for the miR-2* strand and related proteins accumulation as observed in *alg-1(anti)* mutants by (*C*) ALG-1(anti) IP and (*D*) miR-2 and miR-2* 2′O-methyl pull-downs.

ALG-1 Argonaute both disrupt miRLC to miRISC maturation but impose distinct effects on the ability of ALG-1 to interact with specific microRNA and protein cofactors.

Distinct Effects of ALG-1(anti) on Different microRNAs. Our data indicate at least two distinct effects of ALG-1(anti) on microRNA biogenesis that are exhibited to varying degrees by different microRNAs: loss of specificity of guide strand selection (for example, mir-2) (Table 1), and defective passenger strand release (for example: mir-58) (Table 1). At this point we cannot estimate how many microRNAs in classes I and II/III could be defective in only passenger strand release (such as mir-58), or only guide strand selection, or could be affected by compound defects in both processes.

We speculate that differing effects of ALG-1(anti) on miR strand selection and miR* disposal for distinct microRNAs could reflect how ALG-1 recognizes sequence-specific or duplex structure-specific features characteristic of each pre-microRNA in the context of miRLC. Presumably, for all microRNAs, guide strand selection involves a sampling by the miRLC of both orientations of the duplex (with either miR or miR* sampled as the potential guide), with the specificity of the guide strand choice determined by mechanisms that couple passenger release selectively to a specific duplex orientation (Fig. 6). There is evidence that microRNA passenger strand selection by Argonaute may involve conformational changes in the Argonaute::pre-mir complex that could be triggered by structural features characteristic of one duplex orientation, and that subsequently favor passenger strand release (19). It is possible that ALG-1(anti) mutant proteins are primarily defective in key miRLC conformational changes that couple miR* or passenger strand release to a specific duplex orientation for specific microRNAs. According to this model, microRNAs, such as mir-2 and other class I asymmetric microRNAs, correspond to cases where strand selection depends on a conformational change that is defective in ALG-1(anti). On the other hand, microRNAs (such as mir-58) that display proper strand selection in *alg-1(anti)* mutants, but poor miR* strand release, are those for which strand selection is determined before the defective conformational change.

Interestingly, the class of asymmetric microRNAs, whose miR* strands were more abundant in the ALG-1(anti) than their miR strands (class I in Table 1), is enriched for microRNAs with paired duplex ends at both the 5′ and the 3′ ends (Fig. S7*E*), with all of the asymmetric microRNA duplexes being paired at the 3′ end. At the same time, the majority of the unaffected microRNAs had an unpaired 3′ nucleotide (Fig. S7*E*). This observation is intriguing but not predictive of asymmetric loading, as that difference alone cannot explain the disparity between miR* Argonaute loading for class I microRNAs compared with all other microRNAs. It is possible that our inability to identify microRNA duplex features as predictors of asymmetric loading into ALG-1(anti) was hampered by the small sample size of class I microRNAs in this study (Table 1). Therefore, we do not preclude the possibility that certain features or some combination thereof may in fact influence strand loading in *alg-1(anti)* mutants. However, our data raise an intriguing possibility that additional microRNA-extrinsic mechanisms may help determine which microRNA strand becomes loaded and functional.

It's interesting to consider that different rules governing guide strand selection and passenger disposal may apply to different

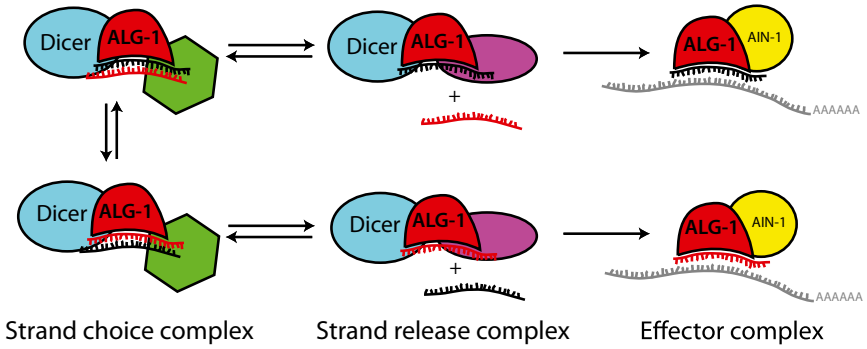

Fig. 6. A model representing factors that influence the orientation of microRNA duplex loading.

microRNAs. Given the differences between protein cofactors associated with ALG-1 in wild-type and *alg-1(anti)* mutant animals, one attractive possibility is that Argonaute cofactors may be what imparts the context/microRNA specificity of strand selection and allows for modulation of strand choice (Fig. 6). We suggest that duplex orientation is sampled by the miRLC and that loading of the duplex into the Argonaute in correct orientation depends on several properties, both intrinsic and extrinsic to the microRNA duplex itself. We propose that features of the duplex structure, conformation of the Argonaute protein itself, and the presence of microRNA-specific protein cofactors (shown in green and purple in Fig. 6) may all be important for the appropriate orientation of the duplex during miRLC loading.

Given the evidence that passenger strand may be functional in certain circumstances (23, 44–46), the ability to modulate the choice between guide and passenger strands must be highly regulated. Such regulation could be indispensable in developmental and pathological contexts in which the specificity of guide/passenger strand selection is critical. Further study is required to develop a fuller understanding of how microRNA strand choice is executed and regulated by Argonautes and their associated cofactors.

ACKNOWLEDGMENTS. We thank the members of the V.R.A. and the Mello laboratories for helpful discussions, especially Weifeng Gu for help with initial high-throughput sequencing data analysis; and the University of Massachusetts Medical School Molecular Biology Core for performing the high-throughput sequencing. This work was supported in part by a Tara Bean postdoctoral fellowship (to A.Y.Z.); a Leukemia and Lymphoma Society postdoctoral fellowship (to I.V.-L.); and National Institutes of Health Grants R01GM089778 (to J.A.W.) and R01GM34028 (to V.R.A.).

1. Friedman RC, Farh KK-H, Burge CB, Bartel DP (2009) Most mammalian mRNAs are conserved targets of microRNAs. *Genome Res* 19(1):92–105.
2. Maniataki E, De Planell Saguer MDA, Mourelatos Z (2005) Immunoprecipitation of microRNPs and directional cloning of microRNAs. *Methods Mol Biol* 309:283–294.
3. Liu X, Jin D-Y, McManus MT, Mourelatos Z (2012) Precursor microRNA-programmed silencing complex assembly pathways in mammals. *Mol Cell* 46(4):507–517.
4. Iwasaki S, et al. (2015) Defining fundamental steps in the assembly of the *Drosophila* RNAi enzyme complex. *Nature* 521(7553):533–536.
5. Martinez NJ, Chang H-M, Borrajo J de R, Gregory RI (2013) The co-chaperones Fkbp4/5 control Argonaute2 expression and facilitate RISC assembly. *RNA* 19(11):1583–1593.
6. Iwasaki S, et al. (2010) Hsc70/Hsp90 chaperone machinery mediates ATP-dependent RISC loading of small RNA duplexes. *Mol Cell* 39(2):292–299.
7. Meister G (2013) Argonaute proteins: Functional insights and emerging roles. *Nat Rev Genet* 14(7):447–459.
8. Miki TS, Rüegger S, Gaidatzis D, Stadler MB, Großhans H (2014) Engineering of a conditional allele reveals multiple roles of XRN2 in *Caenorhabditis elegans* development and substrate specificity in microRNA turnover. *Nucleic Acids Res* 42(6):4056–4067.
9. Warf MB, Johnson WE, Bass BL (2011) Improved annotation of *C. elegans* microRNAs by deep sequencing reveals structures associated with processing by Drosha and Dicer. *RNA* 17(4):563–577.
10. Okamura K, Liu N, Lai EC (2009) Distinct mechanisms for microRNA strand selection by *Drosophila* Argonautes. *Mol Cell* 36(3):431–444.
11. Czech B, et al. (2009) Hierarchical rules for Argonaute loading in *Drosophila*. *Mol Cell* 36(3):445–456.
12. Ghildiyal M, Xu J, Seitz H, Weng Z, Zamore PD (2010) Sorting of *Drosophila* small silencing RNAs partitions microRNA* strands into the RNA interference pathway. *RNA* 16(1):43–56.
13. Seitz H, Tushir JS, Zamore PD (2011) A 5′-uridine amplifies miRNA/miRNA* asymmetry in *Drosophila* by promoting RNA-induced silencing complex formation. *Silence* 2:4.
14. Frank F, Sonenberg N, Nagar B (2010) Structural basis for 5′-nucleotide base-specific recognition of guide RNA by human AGO2. *Nature* 465(7299):818–822.
15. Mi S, et al. (2008) Sorting of small RNAs into *Arabidopsis* Argonaute complexes is directed by the 5′ terminal nucleotide. *Cell* 133(1):116–127.
16. Khvorova A, Reynolds A, Jayasena SD (2003) Functional siRNAs and miRNAs exhibit strand bias. *Cell* 115(2):209–216.
17. Schwarz DS, et al. (2003) Asymmetry in the assembly of the RNAi enzyme complex. *Cell* 115(2):199–208.
18. Krol J, et al. (2004) Structural features of microRNA (miRNA) precursors and their relevance to miRNA biogenesis and small interfering RNA/short hairpin RNA design. *J Biol Chem* 279(40):42230–42239.
19. Kawamata T, Seitz H, Tomari Y (2009) Structural determinants of miRNAs for RISC loading and slicer-independent unwinding. *Nat Struct Mol Biol* 16(9):953–960.
20. Yoda M, et al. (2010) ATP-dependent human RISC assembly pathways. *Nat Struct Mol Biol* 17(1):17–23.
21. Hu HY, et al. (2009) Sequence features associated with microRNA strand selection in humans and flies. *BMC Genomics* 10:413.
22. Wang Y, et al. (2014) The expression of miR-30a* and miR-30e* is associated with a dualistic model for grading ovarian papillary serious carcinoma. *Int J Oncol* 44(6):1904–1914.
23. Bang C, et al. (2014) Cardiac fibroblast-derived microRNA passenger strand-enriched exosomes mediate cardiomyocyte hypertrophy. *J Clin Invest* 124(5):2136–2146.
24. Yang J-S, et al. (2011) Widespread regulatory activity of vertebrate microRNA* species. *RNA* 17(2):312–326.
25. Okamura K, et al. (2008) The regulatory activity of microRNA* species has substantial influence on microRNA and 3′ UTR evolution. *Nat Struct Mol Biol* 15(4):354–363.
26. Wilson RC, et al. (2015) Dicer-TRBP complex formation ensures accurate mammalian microRNA biogenesis. *Mol Cell* 57(3):397–407.
27. Nishida KM, et al. (2013) Roles of R2D2, a cytoplasmic D2 body component, in the endogenous siRNA pathway in *Drosophila*. *Mol Cell* 49(4):680–691.
28. Betancur JG, Tomari Y (2012) Dicer is dispensable for asymmetric RISC loading in mammals. *RNA* 18(1):24–30.
29. Murchison EP, Partridge JF, Tam OH, Cheloufi S, Hannon GJ (2005) Characterization of Dicer-deficient murine embryonic stem cells. *Proc Natl Acad Sci USA* 102(34):12135–12140.
30. Suzuki HI, et al. (2015) Small-RNA asymmetry is directly driven by mammalian Argonautes. *Nat Struct Mol Biol* 22(7):512–521.
31. Zinovyeva AY, Bouasker S, Simard MJ, Hammell CM, Ambros V (2014) Mutations in conserved residues of the *C. elegans* microRNA Argonaute ALG-1 identify separable functions in ALG-1 miRISC loading and target repression. *PLoS Genet* 10(4):e1004286.
32. Brenner S (1974) The genetics of *Caenorhabditis elegans*. *Genetics* 77(1):71–94.
33. Lee RC, Hammell CM, Ambros V (2006) Interacting endogenous and exogenous RNAi pathways in *Caenorhabditis elegans*. *RNA* 12(4):589–597.
34. Lee RC, Ambros V (2001) An extensive class of small RNAs in *Caenorhabditis elegans*. *Science* 294(5543):862–864.
35. Gu W, Claycomb J, Batista P, Mello C, Conte D (2011) *Methods in Molecular Biology*, eds Hobman TC, Duchaine TF (Humana Press, Totowa, NJ), pp 251–280.
36. Jannot G, Vasquez-Rifo A, Simard MJ (2011) *Methods in Molecular Biology*, eds Hobman TC, Duchaine TF (Humana Press, Totowa, NJ), pp 233–249.
37. Huntzinger E, et al. (2013) The interactions of GW182 proteins with PABP and deadenylases are required for both translational repression and degradation of miRNA targets. *Nucleic Acids Res* 41(2):978–994.
38. Kuzuoglu-Öztürk D, Huntzinger E, Schmidt S, Izaurralde E (2012) The *Caenorhabditis elegans* GW182 protein AIN-1 interacts with PAB-1 and subunits of the PAN2-PAN3 and CCR4-NOT deadenylase complexes. *Nucleic Acids Res* 40(12):5651–5665.
39. Braun JE, Huntzinger E, Izaurralde E (2012) A molecular link between miRISCs and deadenylases provides new insight into the mechanism of gene silencing by microRNAs. *Cold Spring Harb Perspect Biol* 4(12):4.
40. Vasquez-Rifo A, et al. (2012) Developmental characterization of the microRNA-specific *C. elegans* Argonautes alg-1 and alg-2. *PLoS One* 7(3):e33750.
41. Corrêa RL, Steiner FA, Berezikov E, Ketting RF (2010) MicroRNA-directed siRNA biogenesis in *Caenorhabditis elegans*. *PLoS Genet* 6(4):e1000903.
42. Landgraf P, et al. (2007) A mammalian microRNA expression atlas based on small RNA library sequencing. *Cell* 129(7):1401–1414.
43. Bouasker S, Simard MJ (2012) The slicing activity of miRNA-specific Argonautes is essential for the miRNA pathway in *C. elegans*. *Nucleic Acids Res* 40(20):10452–10462.
44. Kozomara A, Hunt S, Ninova M, Griffiths-Jones S, Ronshaugen M (2014) Target repression induced by endogenous microRNAs: Large differences, small effects. *PLoS One* 9(8):e104286.
45. Ji H, et al. (2014) Deep sequencing of RNA from three different extracellular vesicle (EV) subtypes released from the human LIM1863 colon cancer cell line uncovers distinct miRNA-enrichment signatures. *PLoS One* 9(10):e110314.
46. Almeida MI, et al. (2012) Strand-specific miR-28-5p and miR-28-3p have distinct effects in colorectal cancer cells. *Gastroenterology* 142(4):886–896.e9.
47. Zou Y, et al. (2013) Developmental decline in neuronal regeneration by the progressive change of two intrinsic timers. *Science* 340(6130):372–376.
48. Langmead B, Trapnell C, Pop M, Salzberg SL (2009) Ultrafast and memory-efficient alignment of short DNA sequences to the human genome. *Genome Biol* 10(3):R25.
49. Kozomara A, Griffiths-Jones S (2014) miRBase: Annotating high confidence microRNAs using deep sequencing data. *Nucleic Acids Res* 42(Database issue):D68–D73.
50. Kaiser P, Wohlschlegel J (2005) Identification of ubiquitination sites and determination of ubiquitin-chain architectures by mass spectrometry. *Methods Enzymol* 399:266–277.
51. Wohlschlegel JA (2009) Identification of SUMO-conjugated proteins and their SUMO attachment sites using proteomic mass spectrometry. *Methods Mol Biol* 497:33–49.
52. Kelstrup CD, Young C, Lavallee R, Nielsen ML, Olsen JV (2012) Optimized fast and sensitive acquisition methods for shotgun proteomics on a quadrupole orbitrap mass spectrometer. *J Proteome Res* 11(6):3487–3497.
53. Michalski A, et al. (2011) Mass spectrometry-based proteomics using Q Exactive, a high-performance benchtop quadrupole orbitrap mass spectrometer. *Mol Cell Proteomics* 10(9):M111.011015.
54. Cociorva D, Tabb DL, Yates JR (2006) Validation of tandem mass spectrometry database search results using DTASelect. *Curr Protoc Bioinformatics* Chapter 13:Unit 4.
55. Tabb DL, McDonald WH, Yates JR, 3rd (2002) DTASelect and contrast: Tools for assembling and comparing protein identifications from shotgun proteomics. *J Proteome Res* 1(1):21–26.
56. Xu T, et al. (2006) ProLuCID, a fast and sensitive tandem mass spectra-based protein identification program. *Mol Cell Proteomics*, 5(10 suppl):S174.
57. Elias JE, Gygi SP (2007) Target-decoy search strategy for increased confidence in large-scale protein identifications by mass spectrometry. *Nat Methods* 4(3):207–214.
58. Florens L, et al. (2006) Analyzing chromatin remodeling complexes using shotgun proteomics and normalized spectral abundance factors. *Methods* 40(4):303–311.
59. Lorenz R, et al. (2011) ViennaRNA Package 2.0. *Algorithms Mol Biol* 6:26.